

<https://doi.org/10.1038/s43247-025-02341-x>

Climate change-induced amplification of extreme temperatures in large lakes



Hazem U. Abdelhady^{1,2}✉, Ayumi Fujisaki-Manome¹ , David Cannon¹, Andrew Gronewold² & Jia Wang³

Lake surface temperature extremes have shifted over recent decades, leading to significant ecological and economic impacts. Here, we employed a hydrodynamic-ice model, driven by climate data, to reconstruct over 80 years of lake surface temperature data across the world's largest freshwater bodies. We analyzed lake surface temperature extremes by examining changes in the 10th and 90th percentiles of the detrended lake surface temperature distribution, alongside heatwaves and cold-spells. Our findings reveal a 20–60% increase in the 10 and 90 percentiles detrended lake surface temperature in the last 50 years relative to the first 30 years. Heatwave and cold-spell intensities, measured via annual degree days, showed strong coherence with the Arctic Oscillation (period: 2.5 years), Southern Oscillation Index (4 years), and Pacific Decadal Oscillation (6.5 years), indicating significant links between lake surface temperature extremes and both interannual and decadal climate teleconnections. Notably, heatwave and cold-spell intensities for all lakes surged by over 100% after 1996 or 1976, aligning with the strongest El-Niño and a major shift in the Pacific Decadal Oscillation, respectively, marking potential regional climate tipping points. This emphasizes the long-lasting impacts of climate change on large lake thermodynamics, which cascade through larger ecological and regional climate systems.

Lake surface temperature (LST) extremes can significantly impact aquatic and terrestrial ecosystems^{1–3}. Unlike the gradual long-term increase in global mean surface temperature, these events often arise abruptly, leaving little time for both human and natural systems to adapt^{1,4}. Such events can lead to widespread species mortality, rapid long-distance range shifts, decreased aquaculture production in commercial fisheries, and even political tension over shared water bodies^{1,2,4,5}. Over the past few decades, the frequency, duration, and intensity of LST extremes have increased^{1,3}, with projections indicating further intensification in the future^{6,7}. These findings collectively underscore the urgent need to study the evolution of LST extremes, including their amplification over time, within the context of a warming, yet increasingly variable, climate.

Tracking changes in LST extremes can be achieved by monitoring the distribution tails of LST over time, commonly using the 10th and 90th percentiles^{8,9}. These percentile temperatures can also be used to define cold-spells and heatwaves, which further require a minimum duration constraint (e.g., 5 days or more)^{8,10}. Seasonally varying thresholds, whether daily or monthly, are often recommended to account for seasonal variations in extremes and to maintain consistency with atmospheric heatwave definitions⁹. However, it is crucial to distinguish between internal changes in

variability and long-term externally forced temperature trends, which only shift the center of the distribution, resulting in an overall increase in variance^{10–13}. This can be achieved by detrending the LST data to remove long-term changes, thereby correcting for distribution shifts and apparent increases in variability, and then using the detrended temperatures for extreme event calculations^{10,13} (Fig. 1a). Both linear and nonlinear trends have been utilized for detrending ocean and lake temperature data, with recent studies advocating for nonlinear trend methods due to clear evidence of nonlinearity in surface temperature data^{8,14,15}.

Among Earth's largest inland water bodies, the North American Laurentian Great Lakes are perhaps the most dynamic. These lakes (hereafter referred to as the Great Lakes) constitute the largest collective body of fresh surface water on Earth¹⁶. Unlike many other large lakes, the Great Lakes are not as well monitored or modeled in continental and global lake systems^{17,18}. For example, numerous large lakes worldwide have extensive monitoring systems^{17,19} and can be modeled using general lake models, such as the Freshwater Lake model (FLake)²⁰. However, the Great Lakes typically require a 3D modeling framework due to the large size and highly dynamic nature^{21,22}. In situ monitoring of this massive scale water surface is also not trivial, and the lake-wide scale observations often rely on satellite-based

¹Cooperative Institute for Great Lakes Research, University of Michigan, Ann Arbor, MI, USA. ²School for Environment and Sustainability, University of Michigan, Ann Arbor, MI, USA. ³NOAA, Great Lakes Environmental Research Lab, Ann Arbor, MI, USA. ✉e-mail: huhady@umich.edu

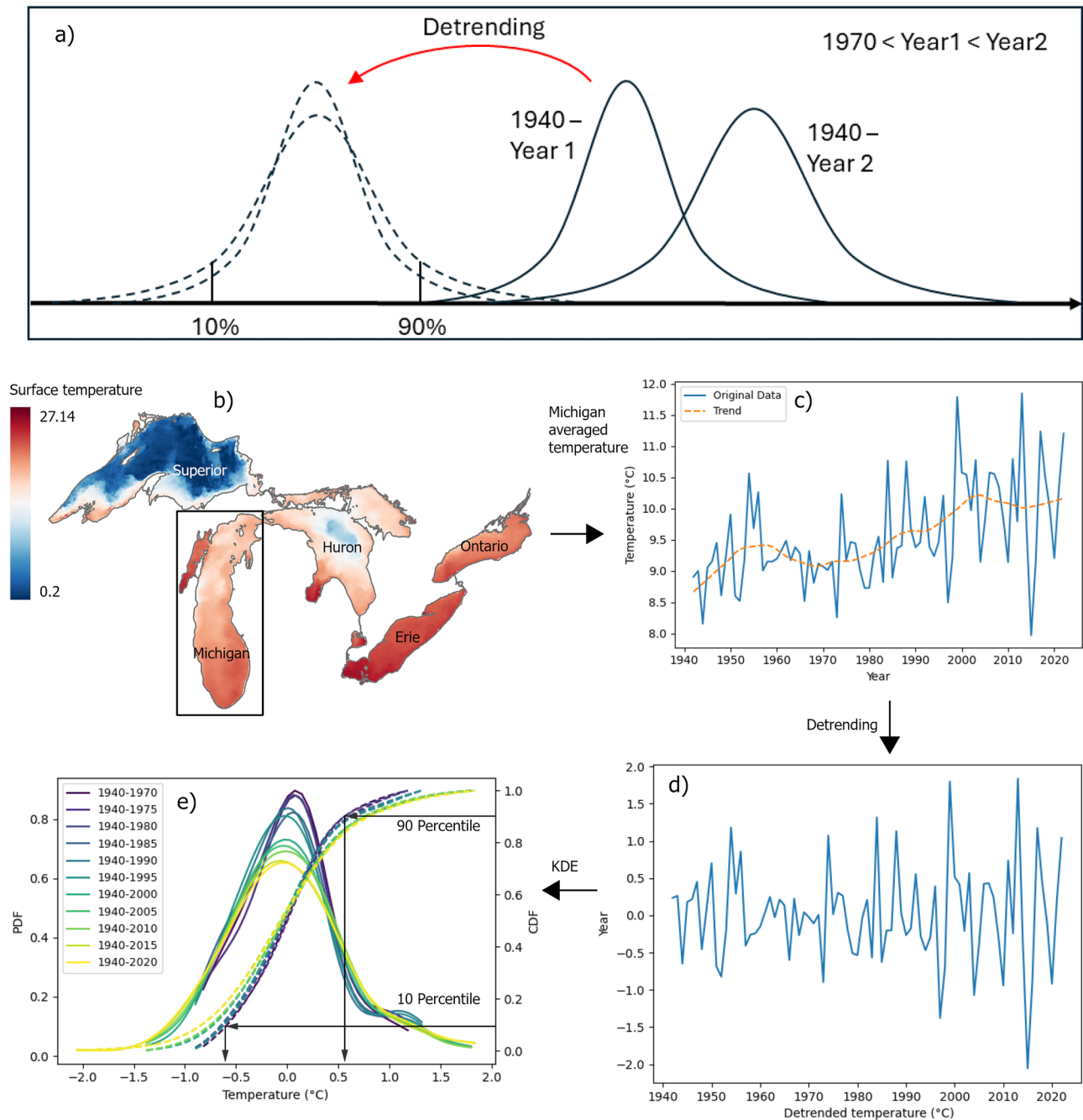


Fig. 1 | Lake surface Temperature detrending and extremes calculation.

a Schematic showing the effect of data detrending on extremes calculations. **b–e** The steps used to calculate the distribution of the detrended lake surface temperature

(DLST). **b** Modeled lake surface temperature (LST) for all lakes. **c** Example lake-wide average surface temperature for Lake Michigan with the detected nonlinear trend. **d** The resulting DLST. **e** The change in the DLST distribution with time.

analysis such as the Great Lakes Surface Environmental Analysis (GLSEA) system (<https://coastwatch.glerl.noaa.gov>).

The Great Lakes are experiencing critical changes in LST^{23–28}, affecting diverse ecosystems, organisms, and human activities^{5,29,30}. Moreover, the Great Lakes significantly influence the regional climate^{31,32}, and rising LST due to global warming is expected to shift regional climate patterns^{26,32}. This has motivated numerous studies to explore changes in Great Lakes water temperatures in the context of climate change, with research utilizing in situ measurements, satellite-based measurements, and/or model-based temperatures^{23–25,33}. However, most of these studies rely on relatively short datasets (25 years or less) due to the limited availability of LST records and the extensive computational resources required for obtaining simulated data. Consequently, these studies have primarily focused on seasonal and

annual changes in mean conditions or have examined temperature extremes, such as heatwaves, over relatively short periods²⁵. This limitation hampers our ability to study the long-term evolution of LST extremes or detect shifts in the thermal structure of the Great Lakes.

In this paper, we utilized a high-resolution three-dimensional hydrodynamic model forced by historical reanalysis data (ERA5³⁴) to generate an extensive record of LST for all Great Lakes from 1940 to 2022. We used this 82-year record of LST to explore the evolution of temperature extremes over time. We started by detrending the water temperature data, removing long-term nonlinear trends using the Seasonal and Trend decomposition with Loess (STL)³⁵, to isolate the global mean temperature increase from internal changes in variability. The detrending process was carried out using the lake-wide average (LWA) surface temperature for each lake, incorporating a

daily-dependent nonlinear trend. We then analyzed the distribution of the detrended LST using a progressive approach, starting with the period from 1941 to 1970 as a reference and incrementally adding five years of data at a time until the entire dataset from 1941 to 2022 was covered. The Kernel Density Estimation (KDE) method was used to estimate the probability density functions of the detrended LST samples. To track the evolution of LST extremes and data spread, we extracted the 10th percentile, 90th percentile, and interquartile range (IQR) from all distributions. Furthermore, we used the detrended daily LST to identify heatwaves and cold-spells, with the 90th and 10th percentiles of the 1941–1970 period serving as references for heatwaves and cold-spells, respectively. We applied breakpoint analysis to detect periods with statistically significant increases in the number of days, temperature anomalies, and degree days of heatwaves and cold-spells. Finally, we used spectrum coherence to explore the periodicities of heatwave and cold-spells in relation to regionally important climate teleconnection indices, including the Oceanic Niño Index (ONI), Arctic Oscillation (AO), Southern Oscillation (SOI), and Pacific Decadal Oscillation (PDO).

Results

A three-dimensional, fully coupled hydrodynamic and ice model was configured for all five Laurentian Great Lakes using the Finite Volume Community Ocean Model (FVCOM) coupled with the Los Alamos Sea Ice Model (CICE) (see Methods). LST results from the hydrodynamic-ice model simulations were compared to Great Lakes Surface Environmental Analysis (GLSEA) surface temperature data available for the years 1995 to 2022. The modeled LST showed strong agreement with the GLSEA data across all lakes, accurately capturing both seasonal and interannual variability. The root mean square error (RMSE) for all daily lake-averaged surface temperatures ranged between 0.89 and 1.58 °C, with Lake Superior (the deepest and the northernmost among the five Great Lakes) exhibiting the largest RMSE and Lake Erie (the shallowest and the southernmost among the five Great Lakes) the smallest. Bias in the simulated surface temperatures ranged between −0.51 and 0.32 °C, with Lake Huron and Lake Superior showing the smallest and largest absolute bias, respectively. These results demonstrate the model's robustness and reliability in reproducing observed surface temperature patterns, thereby validating its use for further exploration of temperature extremes and their evolution over time (see Methods for additional details on model validation).

Nonlinear Detrending and Distribution Changes

The detrending analysis (see Methods) of the LST time series resulted in nonlinear long-term trend and detrended LST (DLST) (Fig. 1). Overall, the nonlinear long-term trends for all lakes demonstrate an increase in LST alongside a low-amplitude multidecadal cycle (Supplementary Fig. 1). The temporal evolution of the DLST distribution was calculated sequentially by adding 5 years at a time to the base period from 1941 to 1970 and recalculating the distribution (see Methods), resulting in a series of DLST distributions for yearly (Fig. 2) and monthly-averaged data (Fig. 3, and Supplementary Figs. 2, 3, 4, 5). All the yearly averaged DLST distributions showed a substantial increase in variability, evident in the attenuation of the distribution peaks and the widening of the tails. The increase in spread, quantified using the interquartile range (IQR), was notable for all lakes from 1970 to 2022 compared to the base period (Fig. 4 and Table 1). The increase in the IQR of the yearly average DLST ranged between 25% and 43%, with Lake Huron (Ontario) showing the largest (smallest) percentage increase.

The monthly distribution analysis highlighted the seasonal variability of DLST for each lake (Fig. 3, and Supplementary Figs. 2, 3, 4, 5). Changes in the monthly distributions were more diverse than the yearly changes, with some months showing increases, decreases, or constant variability. Generally, May, June, and July exhibited the largest range of DLST (i.e., highest variability), while December, January, and February showed the smallest range. All lakes experienced the greatest increase in IQR from 1970 to 2022 during February, March, April, and May, with some months showing more than a 100% increase in IQR (e.g., Lake Huron in March and Lake Michigan in May) (Supplementary Fig. 6). Conversely, minimal changes in variability

were observed during September, October, and November, with some lakes showing a 10% to 15% decrease in IQR.

Water Temperature Extremes

We tracked the evolution of the 10th and 90th percentiles of the DLST distribution to assess changes in the extremes over time. All lakes showed a substantial increase in the annual low temperature extremes (10th percentile) and high temperature extremes (90th percentile) from 1970 to 2022 (Fig. 4) relative to the reference period 1941–1970. The annual low temperature extremes increased by 22% to 45%, colder low temperatures, with Lake Ontario and Lake Michigan experiencing the largest increases, and Lake Superior and Lake Erie experiencing the smallest increases. Notably, there was an abrupt increase in low extremes after 1995, which accounted for most of the overall increase in the extremes. Similarly, the annual high temperature extremes increased by 20% to 60%, with Lake Ontario and Lake Superior showing the largest and smallest increases, respectively (Table 1).

Despite the general increasing trend of annual low and high temperature extremes, monthly extremes exhibited greater diversity, with different lakes showing varying behaviors. Lake Superior experienced some of the most substantial increases in the relative low temperature extremes during February, March, and April, with increases exceeding 400% in February and March (Supplementary Fig. 7). Conversely, Lake Ontario experienced the least increase in the relative low temperature extremes for most months. The smallest changes in the relative low temperature extremes for all lakes were observed in September, October, and November, with some lakes even showing fewer extremes. Additionally, there was a notable jump in relative low temperature extremes after 1990 during February, May, June, and August.

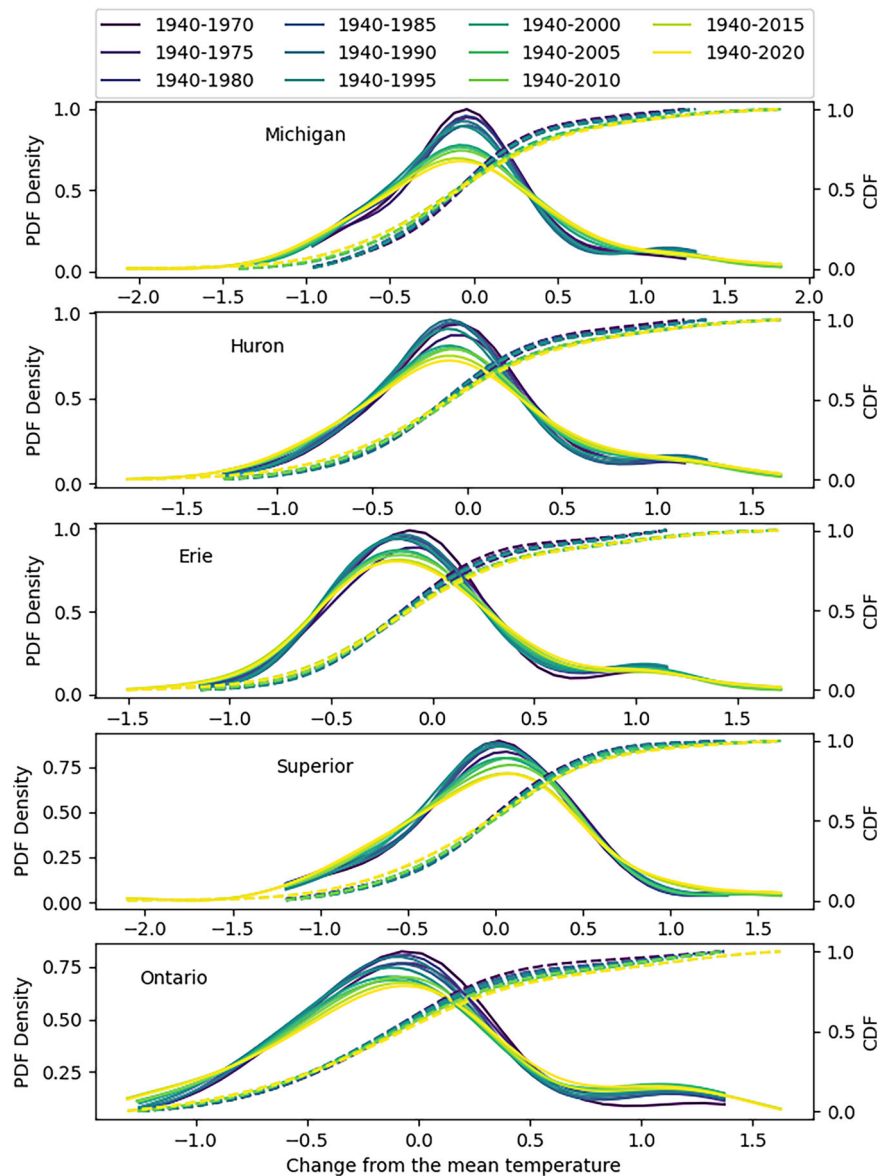
All lakes experienced substantial increases in relative high temperature extremes from December through June, with Lake Superior showing nearly a 300% increase in March and Lake Huron a 175% increase in March (Supplementary Fig. 8). September and November showed decreases in high temperature extremes for some lakes, while July and August remained constant across most lakes. Similarly, some lakes exhibited major jumps in high temperature extremes after 1990, particularly in February, April, and May. For example, Lake Superior gained most of its increase in relative high temperature extremes in February, April, and May after 1995 (Supplementary Fig. 8). Overall, the changes in low and high extremes showed similar seasonal patterns for most of the Lakes.

Heatwaves and Cold-Spells

The number, mean temperature anomaly, and degree heating/cooling days of all detected heatwaves and cold-spells from the daily DLST are presented in Figs. 5 and 6. Breakpoint analysis was used to identify potential breakpoints in the heatwaves and cold-spell intensity time series, and the t-test was employed to assess the statistical significance of these breakpoints (see Methods). Overall, most lakes experienced statistically significant increases in heatwave and cold-spell intensities, based on a 95% significance level (Fig. 7). The mean percentage change in the heatwave intensities ranged between 85% and 258%, with Lake Superior experiencing the largest percentage change and Lake Ontario the smallest (Table 1). The suggested breakpoints for heatwaves across all lakes occurred around 1991 and 1996. The percentage increase in cold-spell intensities ranged between 100% and 168%, with Lake Superior and Lake Ontario experiencing the largest and smallest percentage changes, respectively. Cold-spell intensities showed breakpoints between 1991 and 1996 for Lakes Michigan, Huron, and Superior, while Lakes Ontario and Lake Erie had a different breakpoint around 1976.

In addition to the overarching annual breakpoint analysis, we conducted a monthly analysis to explore the seasonal variability trends. All lakes exhibited statistically significant shifts in degree heating days during January and March (Fig. 5). May and June showed the largest mean changes in degree heating days across all lakes, with Lake Superior experiencing the largest change of 13.1 °C days in June. The period from December to May showed the most substantial increases in the number

Fig. 2 | Changes in yearly averaged detrended lake surface temperature distribution. The change in yearly averaged detrended lake surface temperature (DLST) distribution with time for different Lakes.



of heatwave days, while August to November did not show increasing trends for most lakes. All lakes, except Lake Michigan, exhibited decreasing trends in heatwaves during August and September, both in degree heating days and mean temperature anomaly. The mean temperature anomaly typically increased from December to June and either remained constant or decreased for the rest of the year across all lakes, with Lake Superior experiencing the largest increase during June and July when anomalies exceeded 0.8 °C.

Similarly, we detected a statistically significant increase in the absolute mean of degree cooling days for cold-spells across most months and lakes (Fig. 6). Winter and spring months (December to June) experienced the most substantial increases in cold-spells, with Lake Superior having the highest increase in the absolute mean of degree cooling days, reaching 10 °C days in June. The mean number of days identified as cold-spells increased for most months across all lakes, with February showing an increase of more than 15 cold-spell days after 2000. The mean temperature anomaly of cold-spells also increased for many months across all lakes, with the majority of these increases being statistically significant. Overall, Lake Superior experienced the largest increases in all cold-spell variables, with most changes occurring after 1996. Other lakes exhibited multiple breakpoints, with 1996, 1991, and 1975 being the most notable.

In addition to the overall increase in heatwaves and cold-spells, we observed periodicity in their intensities. Using the Welch method³⁶, we calculated the power spectrum for the yearly degree heating days and degree cooling days, assessing the statistical significance of the spectrum peaks against the 95% red noise spectrum (see Methods). The most predominant and statistically significant cycles for degree heating days were identified at approximately 4 and 2.5 years for most lakes (Fig. 8). The degree cooling days spectrum peaks were more diverse across lakes. Although statistically significant periods were found, the most notable cycles were around 6–6.5 years for Lakes Michigan, Erie, and Superior, around 4 years for Lake Superior, and 2–2.5 years for Lakes Erie and Ontario.

Spectrum coherence was estimated between the intensities of heatwaves/cold-spells and various climate teleconnections (see Methods). The AO and NAO showed dominant and statistically significant coherence with degree heating days around the 2.5-year period for all lakes, while the SOI exhibited strong coherence at the 4-year period (Supplementary Fig. 9). The PDO showed dominant and statistically significant coherence with degree cooling days at the 6–6.5 year period for Lakes Michigan, Erie, and Superior, while the SOI exhibited strong coherence with Lake Superior at the 4-year period, and Lake Erie at the 2–2.5-year period (Supplementary Fig. 10). Although coherence calculations revealed statistically significant peaks at

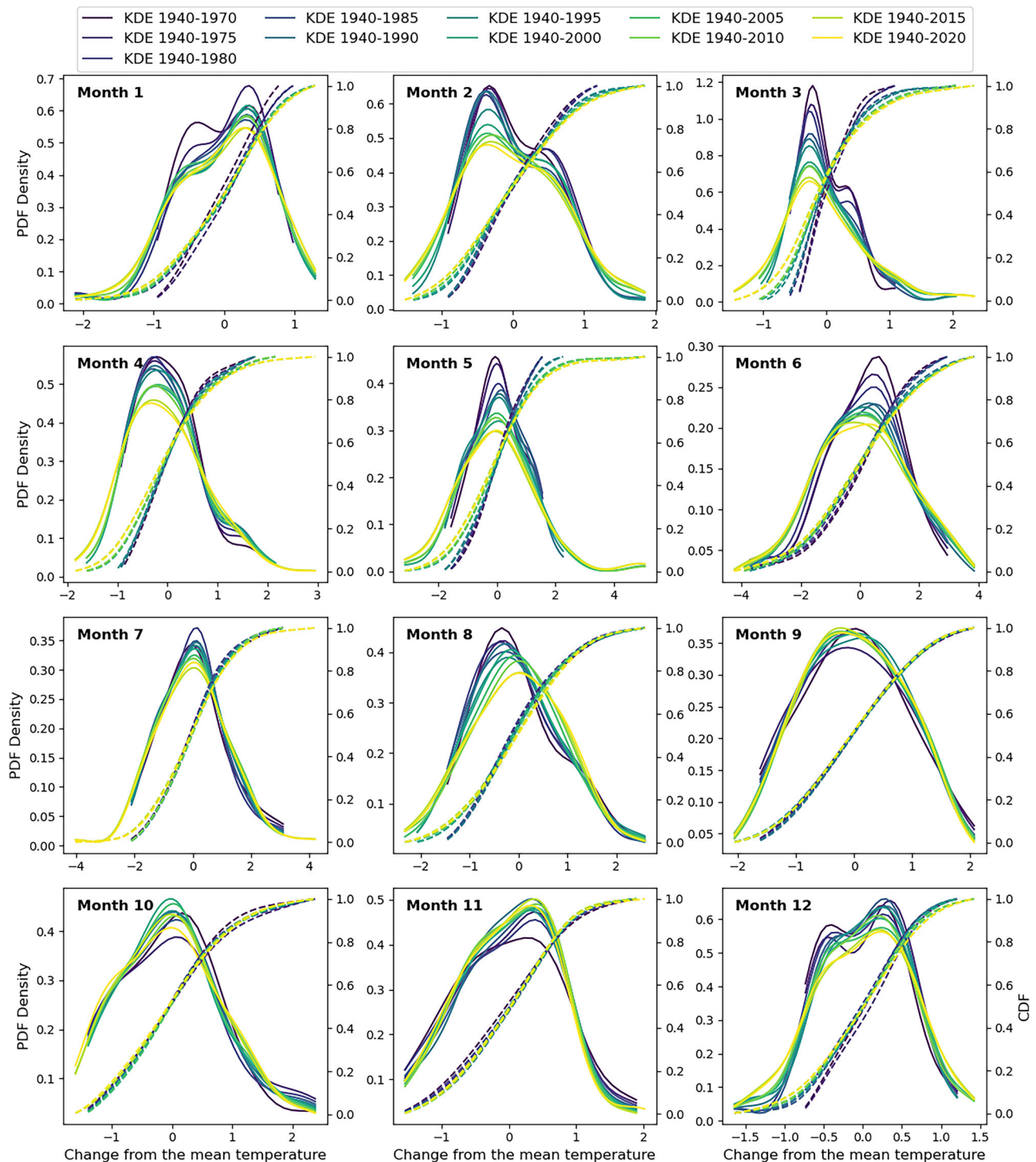


Fig. 3 | Changes in monthly averaged detrended lake surface temperature distribution. The changes in monthly averaged detrended lake surface temperature (DLST) distribution with time for all month for Lake Michigan.

other frequencies, these periods may reflect weak or noisy signals, as they are not accompanied by corresponding significant peaks in the spectra of either the degree heating days or the teleconnection indices.

Discussion

This study highlights the impact of historical climate change on surface temperature extremes across all the Great Lakes. Both low and high surface temperature extremes were observed to be increasing after detrending the surface temperature time series. A significant shift in the degree days of heatwaves and cold-spells was noted for most lakes post-1990s.

Additionally, we observed clear interannual periodicity in the intensities of heatwaves and cold-spells, with significant coherence to the Arctic Oscillation (AO), the Southern Oscillation Index (SOI), and Pacific Decadal Oscillation (PDO) climate teleconnection patterns.

Nonlinear detrending of the surface temperatures was essential to distinguish the increase in variability due to long-term temperature changes from internal variability. The nonlinear trends identified across all lakes accounted for 21% to 39% of the total variance in surface temperatures, representing multi-decadal cycles superimposed on a long-term linear increase. The nonlinear trends show a strong correlation with Atlantic

Fig. 4 | Changes in the detrended lake surface temperature statistics relative to the period of 1941–1970. Time series of the relative 10 percentile, 90 percentile, and IQR for the yearly averaged DLST distribution with time for all lakes.

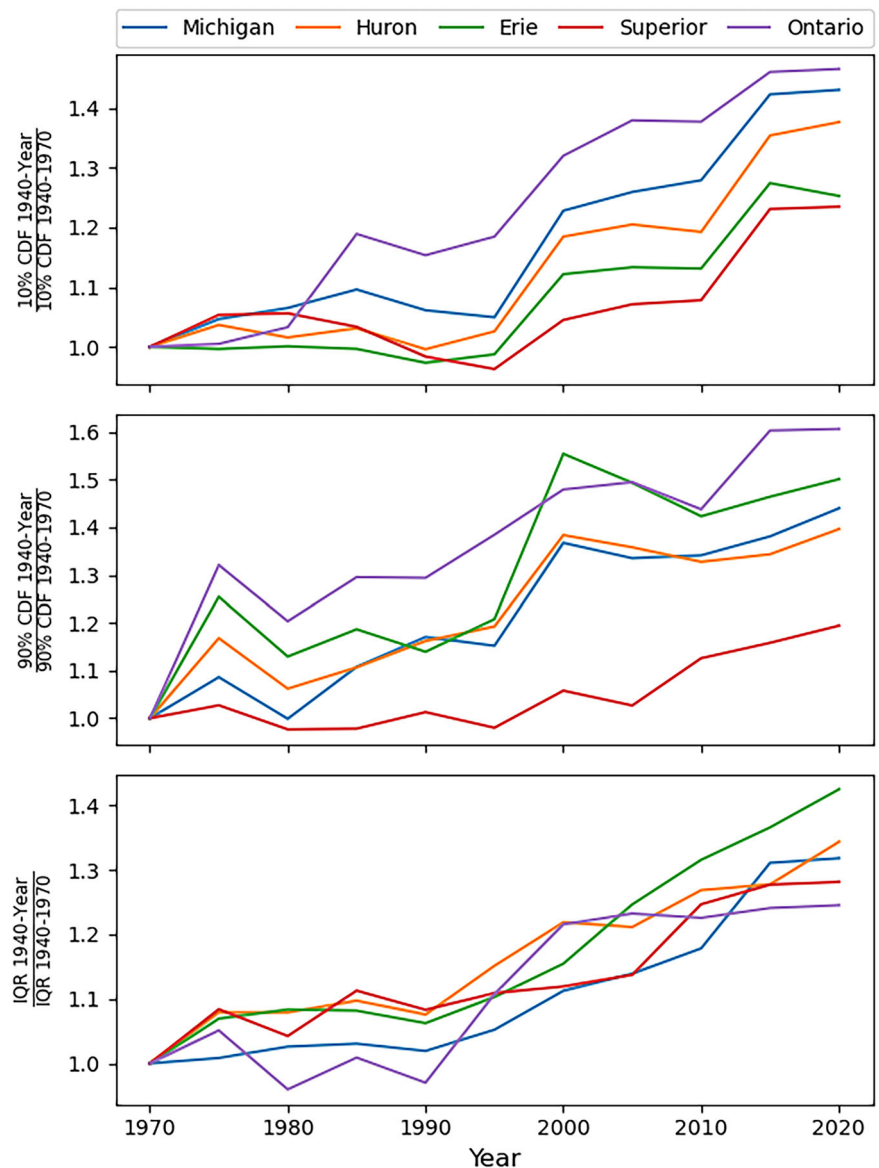


Table 1 | Changes in annual LST variability and extremes

Metric	Michigan	Huron	Erie	Superior	Ontario
IQR % increase	31	34	42	28	24
Std % increase	46	32	31	25	38
10 percentile % increase	43	38	25	23	47
90 percentile % increase	44	39	50	19	60
Heatwaves % increase	135	142	99	258	85.3
Heatwaves breakpoint year (<i>p</i> -value)	1996 (0.04)	1996 (0.028)	1991 (0.038)	1996 (0.018)	1996 (0.069)
Cold-spells % increase	146	140	165	165	100
Cold-spells breakpoint year (<i>p</i> -value)	1991 (0.023)	1996 (0.02)	1976 (0.038)	1996 (0.025)	1976 (0.011)

Multidecadal Oscillation (AMO), with Spearman correlation coefficients ranging from 0.68 to 0.8 for all lakes. However, the AMO was not explicitly used to interpret the periodicity of heatwaves and cold spells in this study because its variability was largely removed along with the long-term non-linear trend. Additionally, given that AMO has a period of 60–90 years³⁷, the 80-year record is insufficient to identify a signal with a period spanning more than half its length. The overall long-term trend displayed a significant

increase for all lakes, with rates from 0.11 °C to 0.17 °C per decade, with Lake Michigan and Lake Superior showing the largest and smallest increases, respectively.

Despite the general warming trend observed in all lakes, low-temperature extremes are still evident, and their frequency and intensities are significantly increasing (Fig. 7 and Table 1). The most severe cold-spell season for most lakes occurred during 2014–2015, with all lakes

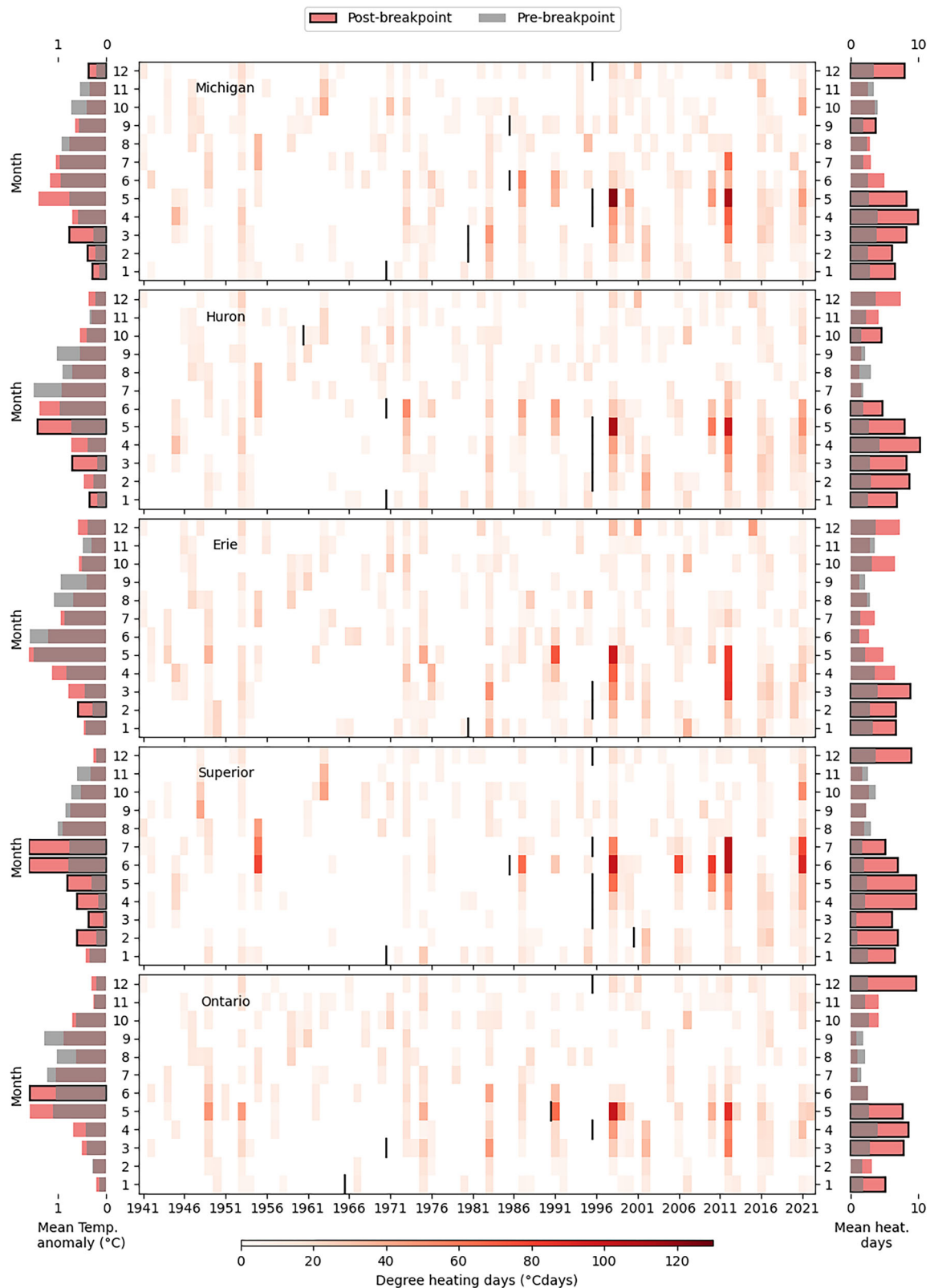


Fig. 5 | Heatwave events from 1941 to 2022. Middle panel shows detected heatwaves for the whole record clustered by month color coded using the degree heating days variable. The short black vertical line indicates the location of the statistically significant breakpoints for each month. Left (Right) column shows the mean

temperature anomaly (the mean heat days or duration of heatwave) for each month before and after the breakpoint. Black squares are used to highlight the statistically significant change in mean temperature anomaly (the mean heat days) before and after the breakpoint. Each row represent a different lake.

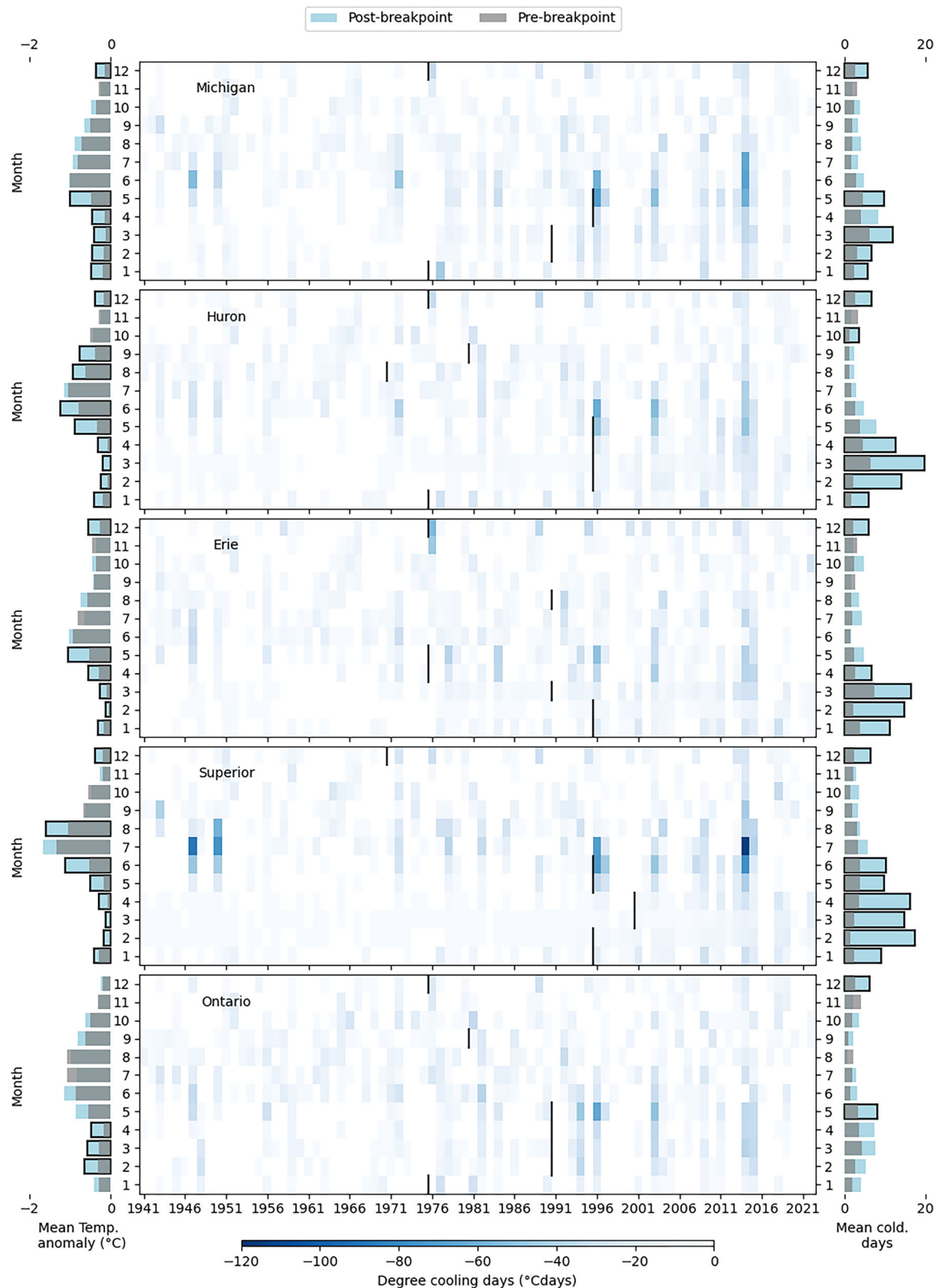


Fig. 6 | Cold-spell events from 1941 to 2022. Middle panel shows detected cold-spells for the whole record clustered by month color coded using the degree cooling days variable. The short black vertical line indicates the location of the statistically significant breakpoints for each month. Left (Right) column shows the mean

temperature anomaly (the mean cool days or duration of cold-spell) for each month before and after the breakpoint. Black squares are used to highlight the statistically significant change in mean temperature anomaly (the mean cool days) before and after the breakpoint. Each row represents a different lake.

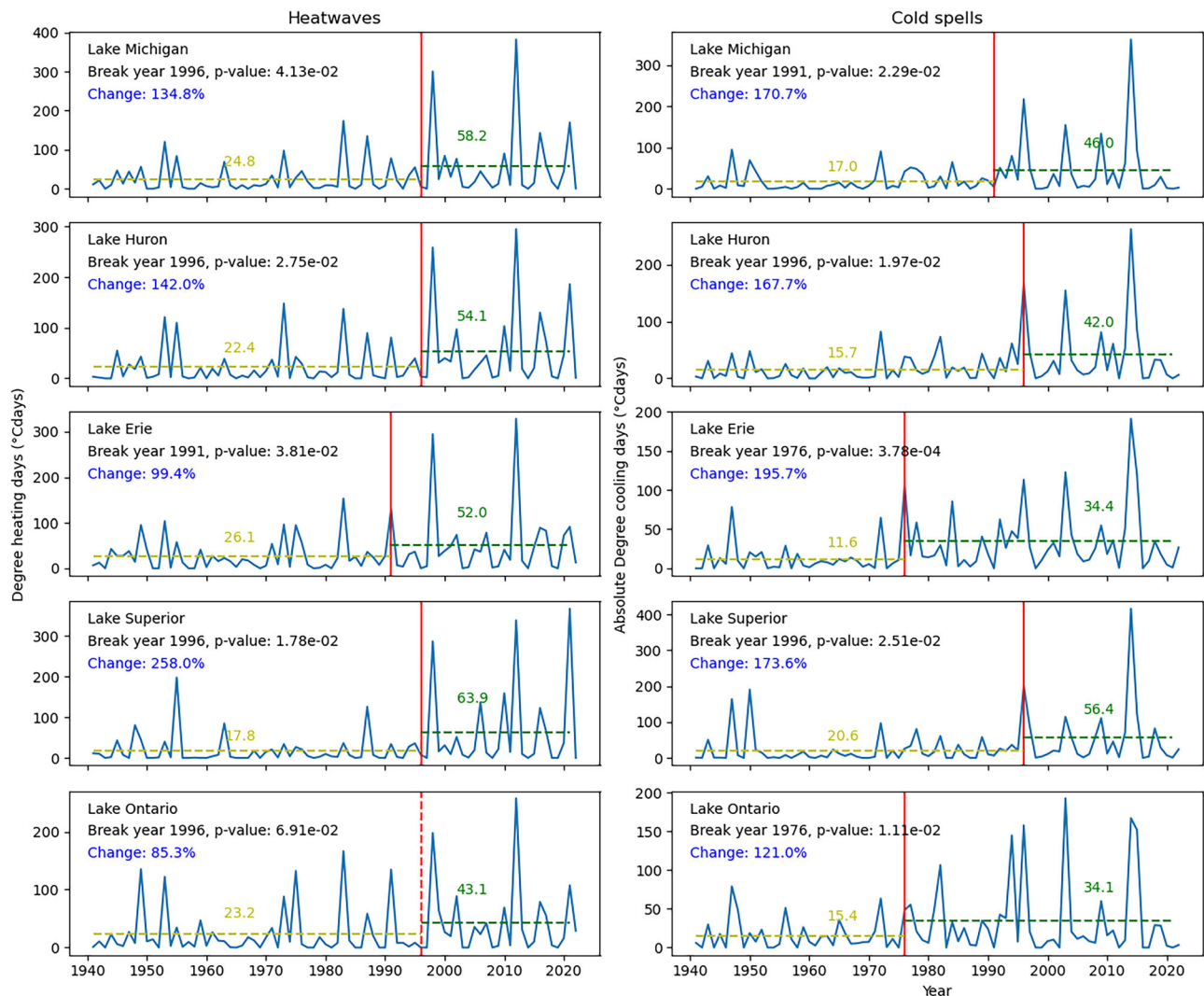


Fig. 7 | Breakpoint analysis for heatwaves and cold-spells for all lakes based on annual degree days. Heatwaves are shown in the left column while cold-spells are shown in the right column. Each row represents a different lake.

experiencing excessive ice cover^{38,39}. Notably, this followed the season with the highest number of heatwaves, 2012–2013, which saw one of the lowest ice cover seasons on record across all lakes. This defines a new level of LST variability in the Great Lakes.

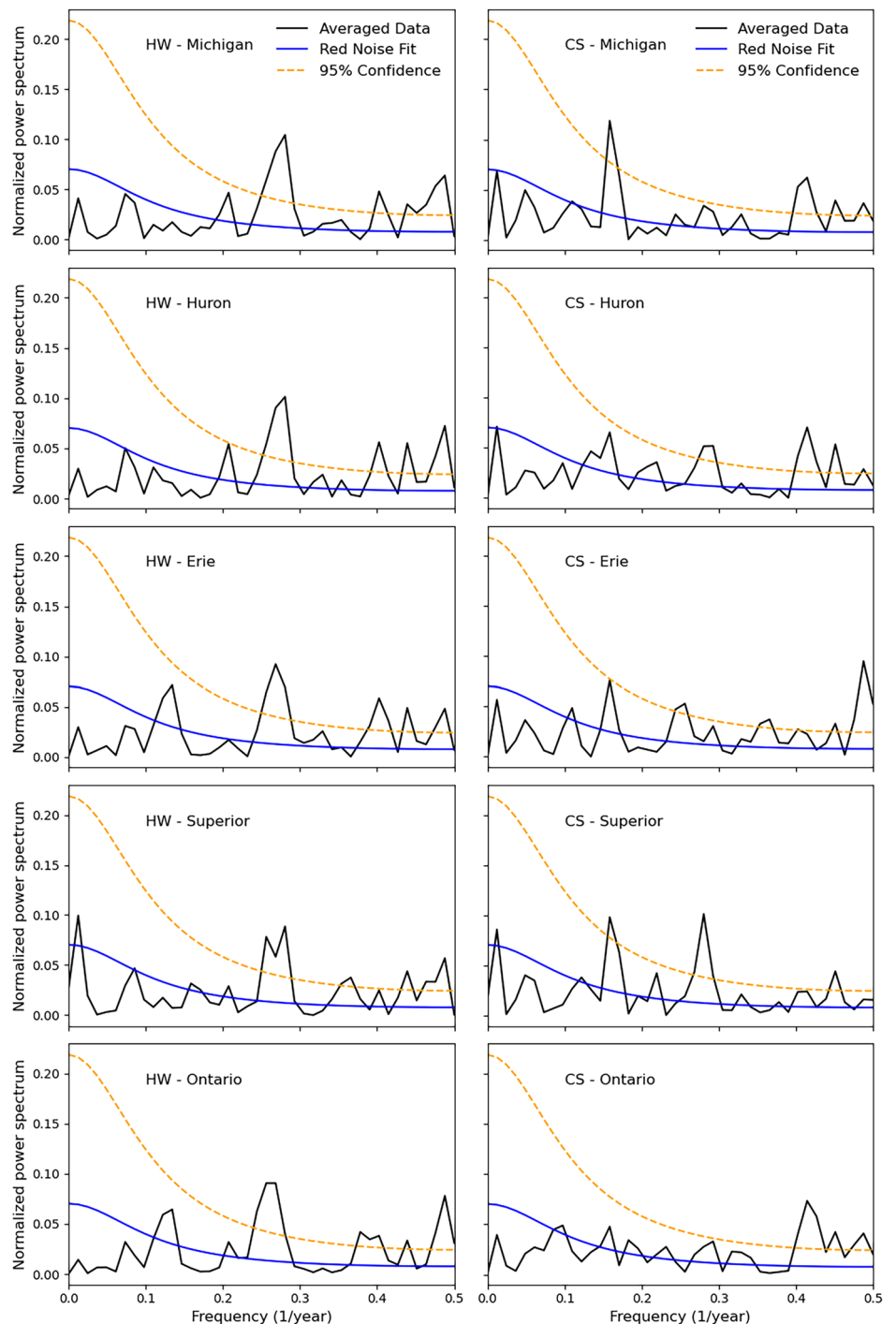
The increase in both low and high detrended surface temperature extremes for all lakes contrasts with observations in ocean surface temperatures, where detrending typically results in relatively constant variance¹⁰. This discrepancy highlights a major difference in the impact of climate change on water surface temperature extremes between the oceans and the Great Lakes. Several factors can explain this difference. The relatively shallow depth and confined nature of the Great Lakes result in a smaller heat capacity, leading to quicker heat absorption and release. In contrast, the deeper, open nature of the ocean, combined with horizontal advection and mesoscale currents, facilitates the redistribution of heat from local heatwaves, thus dampening temperature extremes. Furthermore, the increase in surface air temperature tends to be greater over land than over the ocean, due to the ocean's large thermal inertia⁴⁰. Consequently, the Great Lakes are more directly influenced by extreme continental climate variability and episodic weather patterns, which can induce rapid and significant temperature changes^{24,26,38}. Seasonal ice cover also significantly impacts the thermodynamics of the Great Lakes, reducing absorbed shortwave radiation at the lake surface through the ice/water albedo feedback during winter⁴¹. This variability in ice cover alters the heat budget of the lakes, contributing to temperature variability.

Ice cover primarily drives the seasonal variability of LST extremes. Generally, the first half of the year has seen the most significant increase in both low and high temperature extremes, including heatwaves and cold spells. This trend is largely due to more than a 70% decrease in ice cover over the past 40 years^{42,43}. The reduction in ice cover exposes the lakes to increased solar radiation, raising their heat content and further accelerating ice loss through the positive ice/water albedo feedback⁴¹. Given that ice cover is most extensive during the first half of the year (winter and spring), its reduction and variability directly impact LST during these months. As a result, these months experience a wider range of surface temperatures as time advance, reflected in the increased variability observed compared to the latter half of the year.

Variability in ice cover trends were also linked to spatial variability in LST extremes across the lakes. Heatwave increases were less extreme in lakes with relatively stable ice cover (e.g., Erie: +99%; Ontario: +85%), while lakes with severe ice decline experienced associated increases in heatwaves (e.g., Superior: +258%) (Fig. 7). In Lake Superior, this effect is particularly evident in the emergence of a new peak in May and June in recent years (Supplementary Fig. 3). This pattern likely results from an earlier end to the ice season and an earlier onset of thermal stratification, both of which lead to higher surface temperatures during these months compared to previous decades, contributing to the newly emerging peak^{44,45}.

Results reveal that the periodicity of heatwaves and cold spells is strongly connected to different climate teleconnections, with shifts detected

Fig. 8 | Power spectrum of annual degree days of heatwave and cold-spell for all lakes. Annual degree heating days and degree cooling days are used to calculate heatwaves and cold-spells spectrums, respectively. Heatwaves are shown in the left column while cold-spells are shown in the right column. Each row represents a different lake.



through breakpoint analysis underscoring these relationships. Previous studies find strong connection between AO, NAO, and ONI and ice cover changes in the Great Lakes^{42,46}. Negative (positive) AO/NAO events are often associated with more (less) ice cover, while strong El Niño events are often associated with the least ice cover on the Great Lakes, which support the significance coherence between them. A statistically significant shift in heatwaves was observed around 1996 for most months and lakes, with notable increases in variability across the Great Lakes after the 1990s. This finding is consistent with previous studies reporting similar shifts in water temperature and ice cover in the region^{26,47}. The 1997–1998 El Niño, the strongest winter event on record, likely played a pivotal role, contributing to unusually warm temperatures in the Great Lakes region^{48,49}. This event triggered substantial changes in lake heat content^{33,50}, ice cover⁴⁷, water

levels^{51,52}, and regional climate patterns⁵³. These changes are likely to be attributed to shifts in large-scale atmosphere-ocean patterns. For example⁴⁷, conducted a process-based analysis to show that warm blobs over the northeast Pacific Ocean in recent decades led to eastward shift of the ridge-trough system and resulting increased variability over Great Lakes winter severity and ice cover. Our findings also show a significant rise in temperature extremes and variability since this event, suggesting the occurrence of a regional climate tipping point. These results highlight the highly non-linear response of the Great Lakes system to extreme events and the potential for long-lasting impacts on both lake dynamics and regional climate.

Additionally, the breakpoint analysis identified a shift in cold spells around 1976 for Lake Erie and Lake Ontario (Fig. 7), as well as for select

months in other lakes (Fig. 6). This shift coincides with the transition of the PDO from a negative to positive phase, corresponding to a shift from a warm to cold phase in the Great Lakes region^{38,54}. Notably, the PDO also shows strong spectral coherence with cold-spell intensities for most of the lakes at a periodicity of 6–6.5 years. These observations emphasize the interconnectedness between large-scale climate teleconnections and the variability of extreme events in the Great Lakes, reinforcing that abrupt climatic shifts can have profound and enduring effects on lake dynamics and, by extension, on regional climate patterns and ecosystems.

These findings reinforce the critical necessity of accounting for changes in temperature extremes, in addition to long-term warming, when assessing the impact of climate change on inland water bodies. Our approach provides a clear path for expanding this analysis to other systems, aiding in climate adaptation efforts. Understanding these changes is crucial for developing effective management strategies, particularly in fisheries, habitat restoration, and water quality, where extreme temperature events can influence species distributions, breeding cycles, and harmful algal bloom (HAB) occurrences. Further research is needed to explore how these temperature extremes affect ecosystem dynamics in the Great Lakes, including acute stress on freshwater species and shifts in food web structure. Given the Great Lakes' role in regional climate regulation, freshwater supply, and biodiversity, the implications of our findings highlight how significant changes in these lake systems can cascade through broader ecological and climatic systems.

Methods

Hydrodynamic Model Setup and Validation

Lake physics and thermodynamics were modeled using the Finite Volume Community Ocean Model (FVCOM, version 4.4.2), which employs an unstructured-grid finite volume approach to solve hydrostatic equations²¹. The model domain encompassed all five Laurentian Great Lakes (Superior, Michigan-Huron, Erie, and Ontario) and Lake St. Clair, with an average horizontal spatial resolution of 4.75 km and 21 sigma levels to capture boundary layer processes. The model did not include connecting channels, tributary flows, or groundwater fluxes. A 3D model was chosen over a 1D model because 1D models have been shown to be less accurate for the Great Lakes, given their large spatial extent and depth, often leading to less reliable results than a spatially averaged 3D model^{55–57}. The model was initialized in January 1940 with a uniform temperature of 4 °C and no initial velocity for all cells and sigma layers, running continuously until 2023 with a one-year spin-up period, 1940. The rest of the data from 1941 to 2023 was used for the analysis.

Horizontal turbulence was parameterized using the Smagorinsky scheme, while vertical diffusion utilized the modified Mellor-Yamada level 2.5 turbulent closure scheme. Air-water drag coefficients and heat fluxes were computed using established methods from⁵⁸ and the Coupled Ocean-Atmosphere Response Experiment (COARE)^{59,60}, respectively. Ice dynamics were incorporated using a coupled ice model based on the Los Alamos Sea Ice Model (CICE), which accounted for ice thickness distributions and surface albedo variations⁶¹.

The model was driven by meteorological forcing from the ERA5 reanalysis product, which provides hourly data at about 31 km horizontal resolution for the region³⁴. Surface temperature validation was conducted using data from the Great Lakes Surface Environment Analysis (GLSEA), which offers daily temperature fields with a spatial resolution of approximately 1.3 km, derived from NOAA Advanced Very High Resolution Radar (AVHRR), Visible Infrared Imaging Radiometer Suite onboard the Suomi National Polar-Orbiting Partnership spacecraft (VIIRS S-NPP), and NOAA-20 Visible Infrared Imaging Radiometer Suite (VIIRS NOAA-20).

The model has undergone extensive validation in previous studies. Initially²¹, validated the model by examining circulation patterns and lake surface temperatures. More recently²⁴, further validated the model, focusing on lake surface temperatures and ice cover using remote sensing data from NOAA CoastWatch and reprocessed ice concentration data from⁶². In these assessments, the temperature of the uppermost sigma layer was compared against GLSEA data. Since the model inherently accounts for ice cover,

typically yielding surface temperatures near zero when ice is present, these values were directly used in our calculations of the LST. Additionally²⁴, evaluated the model's performance by comparing simulated and in situ temperature measurements at various depths and locations across the Laurentian Great Lakes. A range of validation metrics, including RMSE, MAE, MBE, CC, and FB, were employed to demonstrate the model's accuracy in replicating observed surface and subsurface conditions. For lake surface temperature, RMSE ranged from 0.89 to 1.58 °C, with a mean bias between -0.51 and 0.32 °C. Ice cover comparisons showed a good match for both seasonal trends and interannual variability with MAE ranges between 4.2% and 13.9%. Vertical profile validation indicated RMSE values generally below 2 °C at most depths, reflecting strong agreement with in situ temperature profiles. For detailed validation results and model limitations, please refer to^{21,22,24}.

Nonlinear Detrending Using STL

To decompose the surface temperature time series and detect the slowly varying nonlinear trends, we employed the non-parametric Seasonal-Trend decomposition procedure based on Loess (STL). STL is a robust and computationally efficient method, commonly used for identifying nonlinear patterns in environmental and climate data^{63–66}. This approach utilizes locally weighted smoothing (Loess) to separate a time series into components representing the long-term trend, seasonal cycle, and residuals^{35,67}. We used the STL function available in the *statsmodels* library in Python⁶⁷. The inputs for the STL model were yearly time series, which included either yearly average surface temperatures or day-of-year (DOY)/monthly temperatures for each year. We used the STL method to calculate the long-term nonlinear trend and subtracted it from the LST data to obtain the detrended LST (DLST) data.

We applied the STL method separately to the DOY data rather than to the entire time series at once. Specifically, we performed the decomposition independently for each calendar day across all years (i.e., 365 separate decompositions) to better capture seasonal variability. This approach mitigates one of the primary challenges of STL in managing nonlinear changes in annual cycles⁶⁶. By doing so, we were able to more accurately distinguish between the seasonally varying long-term nonlinear trend from the internal variability of the time series, leading for better quantification of change in the extremes.

Probability Density Function Estimation

We applied kernel density estimation (KDE) to the DLST to obtain a smooth estimate of the probability density function. We used the *gaussian_kde* function available in the *scipy.stats* library in Python⁶⁸. Since a minimum of 30 years is recommended for studying water temperature extremes⁹, we started with a 30-year baseline period from 1941 to 1970 for calculating KDE. We then appended 5 years at a time to the data and recalculated the KDE to track the evolution of the DLST distribution over time. The analysis was carried out for both yearly averaged data and each month separately to detect the overall changes as well as the seasonal variability. We quantified the increase in the spread of the distribution using the interquartile range (IQR), while the 10th and 90th percentiles were used to track the changes in the extremes.

Heatwaves and cold-spells calculation

Heatwaves are defined as periods when the daily DLST exceeded the seasonally varying 90 percentile threshold for at least five consecutive days, following established criteria by ref. 8. Similarly, cold-spells are defined as periods when the detrended daily mean lake surface temperatures fell below the seasonally varying 10 percentile threshold for at least five consecutive days. Following⁹, a 30-year reference period from 1941 to 1970 was used to calculate the 10 and 90 percentile threshold used for the detection of heatwaves and cold-spells, and these threshold were then applied to the full data from 1941 to 2021. Metrics used to quantify the changes in the detected heatwaves and cold-spells with time are number of days, mean temperature anomaly, and degree heating/

cooling days. In this study, the degree heating/cooling days are used to represent the intensity of heatwaves/cold-spells.

Breakpoint analysis

To identify significant change points in the heatwaves and cold-spells monthly and yearly time series for each lake, we employed a breakpoint analysis using the Binary Segmentation (*Binseg*) approach from the *ruptures* library in Python. The breakpoint detection process was initiated by applying the *Binseg* algorithm with an L2 loss model, which minimizes the sum of squared errors. The algorithm was configured with a minimum segment size of 20 years to avoid detecting spurious change points, and it was allowed to predict only one primary breakpoint.

We tested the statistical significance of the detected breakpoints using the Student's t-test for independent samples. Based on the detected breakpoints, the series was divided into pre- and post-change segments. The t-test was performed using the *ttest_ind* function from the *scipy.stats* library in Python. The p-value derived from this test indicated the likelihood that the difference in means between the pre- and post-change segments occurred by chance, with 5% used as the threshold for the statistical significance.

Spectrum and Coherence Analysis

We conducted the spectral analysis using the Welch method implementation in the *scipy.signal* library in Python⁶⁸. This method segments the time series into overlapping windows, applies a Hann window function to reduce spectral leakage, and averages the resulting periodograms to improve the robustness of spectral estimates⁶⁹. To assess the statistical significance of spectral peaks, we compared them against a theoretical red noise spectrum, which accounts for the inherent autocorrelation in climate time series data^{70,71}. Red noise, often modeled as a first-order autoregressive (AR(1)) process, is characterized by higher power at lower frequencies, reflecting the persistence commonly observed in geophysical processes^{72,73}. We estimated the expected red noise spectrum using a lag-one autocorrelation coefficient ($\alpha = 0.5$), which represents the degree of persistence in the time series. The 95% confidence levels for spectral peaks were determined using the F-statistic, which follows an $F(2, 2)$ distribution due to the two degrees of freedom associated with the spectral estimates⁷⁰. A spectral peak exceeding this threshold indicates a statistically significant departure from red noise behavior, whereas peaks below this level cannot be distinguished from background noise, meaning we fail to reject the null hypothesis that they arise from red noise variability.

We performed spectral coherence analysis between degree heating days and degree cooling days, and several annually averaged teleconnection indices: the Oceanic Niño Index (ONI), North Atlantic Oscillation (NAO), Arctic Oscillation (AO), Southern Oscillation Index (SOI), and Pacific Decadal Oscillation (PDO). Spectral coherence quantifies the strength and phase consistency of shared periodic signals between two time series as a function of frequency. We calculated the spectral coherence using the *multitaper* method, implemented via the *MTCross* class from the *multitaper* package in Python⁷⁴. The multitaper method provides high spectral resolution and reduces leakage by averaging multiple orthogonal taper functions⁷⁵. Statistical significance at the 95% confidence level was assessed using the F-test⁷⁶, with degrees of freedom estimated from the multitaper function. This analysis allowed us to identify significant frequency-dependent relationships between heatwave/cold spell variability and large-scale climate patterns.

Reporting summary

Further information on research design is available in the Nature Portfolio Reporting Summary linked to this article.

Data availability

The data used to run and validate the hydrodynamic model is publicly available. The ERA5 reanalysis climate data used to force the FVCOM model can be downloaded from the Copernicus Climate Data Store (CDS) at [https://cds.climate.copernicus.eu/datasets/reanalysis-era5-pressure-levels?](https://cds.climate.copernicus.eu/datasets/reanalysis-era5-pressure-levels?tab=download)

[tab=download](https://cds.climate.copernicus.eu/datasets/reanalysis-era5-pressure-levels?tab=download). The Great Lakes Surface Environmental Analysis (GLSEA) satellite surface temperature dataset can be accessed from the NOAA CoastWatch Great Lakes Node at <https://coastwatch.glerl.noaa.gov>. The modeled lake surface temperature data are available at <https://doi.org/10.5281/zenodo.15103629>.

Received: 11 December 2024; Accepted: 10 April 2025;

Published online: 15 May 2025

References

1. Till, A., Rypel, A. L., Bray, A. & Fey, S. B. Fish die-offs are concurrent with thermal extremes in north temperate lakes. *Nat. Clim. Change* **9**, 637–641 (2019).
2. Holbrook, N. J. et al. Keeping pace with marine heatwaves. *Nat. Rev. Earth Environ.* **1**, 482–493 (2020).
3. Woolway, R. I. et al. Lake heatwaves under climate change. *Nature* **589**, 402–407 (2021).
4. Smale, D. A. et al. Marine heatwaves threaten global biodiversity and the provision of ecosystem services. *Nat. Clim. Change* **9**, 306–312 (2019).
5. Woodward, G., Perkins, D. M. & Brown, L. E. Climate change and freshwater ecosystems: impacts across multiple levels of organization. *Philos. Trans. R. Soc. B: Biol. Sci.* **365**, 2093–2106 (2010).
6. Yao, Y., Wang, C. & Fu, Y. Global marine heatwaves and cold-spells in present climate to future projections. *Earth's Future* **10**, e2022EF002787 (2022).
7. Huang, L. et al. Emergence of lake conditions that exceed natural temperature variability. *Nat. Geosci.* **17**, 763–769 (2024).
8. Hobday, A. J. et al. A hierarchical approach to defining marine heatwaves. *Prog. Oceanogr.* **141**, 227–238 (2016).
9. Oliver, E. C. et al. Marine heatwaves. *Annu. Rev. Mar. Sci.* **13**, 313–342 (2021).
10. Xu, T. et al. An increase in marine heatwaves without significant changes in surface ocean temperature variability. *Nat. Commun.* **13**, 1–12 (2022).
11. Alexander, M. A., Shin, S. I. & Battisti, D. S. The Influence of the trend, basin interactions, and ocean dynamics on tropical ocean prediction. *Geophys. Res. Lett.* **49**, e2021GL096120 (2022).
12. Wills, R. C., Schneider, T., Wallace, J. M., Battisti, D. S. & Hartmann, D. L. Disentangling Global Warming, Multidecadal Variability, and El Niño in Pacific Temperatures. *Geophys. Res. Lett.* **45**, 2487–2496 (2018).
13. Oliver, E. C. Mean warming not variability drives marine heatwave trends. *Clim. Dyn.* **53**, 1653–1659 (2019).
14. Hartmann, D. L. et al. Observations: atmosphere and surface. *Clim. Change 2013 Phys. Sci. Basis: Working Group I Contribution Fifth Assess. Rep. Intergovernmental Panel Clim. Change* **9781107057999**, 159–254 (2013).
15. Martinez-Lopez, B., Quintanar, A. I., Cabos-Narvaez, W. D. & Moreles, E. On the non-linear nature of long-term sea surface temperature global trends. *Earth Space Sci.* **11**, e2023EA003302 (2024).
16. Shiklomanov, I. *World freshwater resources. In Water in Crisis: A Guide to the World's Fresh Water Resources* (Oxford University Press, 1993).
17. Sorensen, T., Espey, E., Kelley, J. G., Kessler, J. & Gronewold, A. D. A database of in situ water temperatures for large inland lakes across the coterminous United States. *Sci. Data* **2024 11:1** **11**, 1–10 (2024).
18. Balsamo, G. et al. On the contribution of lakes in predicting near-surface temperature in a global weather forecasting model. *Tellus A: Dynamic Meteorology and Oceanography* **64** (2012).
19. Jennings, E. et al. The NETLAKE Metadatabase—“A Tool to Support Automatic Monitoring on Lakes in Europe and Beyond”. *Limnol. Oceanogr. Bull.* **26**, 95–100 (2017).
20. Mironov, D. et al. Implementation of the lake parameterisation scheme FLake into the numerical weather prediction model COSMO. *Boreal Environ. Res.* **15** (2010).

21. Bai, X. et al. Modeling 1993–2008 climatology of seasonal general circulation and thermal structure in the Great Lakes using FVCOM. *Ocean Model.* **65**, 40–63 (2013).
22. Anderson, E. J. et al. Ice forecasting in the next-generation Great Lakes Operational Forecast System (GLOFS). *J. Mar. Sci. Eng.* **6**, 123 (2018).
23. Cannon, D., Fujisaki-Manome, A., Wang, J., Kessler, J. & Chu, P. Modeling changes in ice dynamics and subsurface thermal structure in Lake Michigan-Huron between 1979 and 2021. *Ocean Dyn.* **73**, 201–218 (2023).
24. Cannon, D. et al. Investigating multidecadal trends in ice cover and subsurface temperatures in the Laurentian Great Lakes using a coupled hydrodynamic-ice model. *J. Clim.* **37**, 1249–1276 (2024).
25. Chen, Y. et al. Rapidly expanding lake heatwaves under climate change. *Environ. Res. Lett.* **16**, 094013 (2021).
26. Mason, L. A. et al. Fine-scale spatial variation in ice cover and surface temperature trends across the surface of the Laurentian Great Lakes. *Climatic Change* **138**, 71–83 (2016).
27. Victoria, P. Integrating energy and water resources decision making in the Great Lakes Basin. Tech. Rep., The Great Lakes Commission (2011).
28. Zhong, Y., Notaro, M. & Vavrus, S. J. Spatially variable warming of the Laurentian Great Lakes: an interaction of bathymetry and climate. *Clim. Dyn.* **52**, 5833–5848 (2019).
29. Mandrak, N. E. Potential invasion of the Great lakes by fish species associated with climatic warming. *J. Gt. Lakes Res.* **15**, 306–316 (1989).
30. Lynch, A. J., Taylor, W. W. & Smith, K. D. The influence of changing climate on the ecology and management of selected Laurentian Great Lakes fisheries. *J. Fish. Biol.* **77**, 1764–1782 (2010).
31. Scott, R. W. & Huff, F. A. Impacts of the Great Lakes on Regional climate conditions. *J. Gt. Lakes Res.* **22**, 845–863 (1996).
32. Huang, L. et al. Emerging unprecedented lake ice loss in climate change projections. *Nat. Commun.* **13**, 1–12 (2022).
33. Gronewold, A. D. et al. Impacts of extreme 2013–2014 winter conditions on Lake Michigan’s fall heat content, surface temperature, and evaporation. *Geophys. Res. Lett.* **42**, 3364–3370 (2015).
34. Hersbach, H. et al. The ERA5 global reanalysis. *Q. J. R. Meteorol. Soc.* **146**, 1999–2049 (2020).
35. Cleveland, R. B., Cleveland, W. S., McRae, J. E. & Terpenning, I. STL: A Seasonal-Trend Decomposition. *J. Official Stat.* (1990).
36. Welch, P. D. The use of fast fourier transform for the estimation of power spectra: a method based on time averaging over short, modified periodograms. *IEEE Trans. Audio Electroacoustics* **15**, 70–73 (1967).
37. Knudsen, M. F., Seidenkrantz, M. S., Jacobsen, B. H. & Kuijpers, A. Tracking the Atlantic Multidecadal Oscillation through the last 8,000 years. *Nat. Commun.* **2**, 1–8 (2011).
38. Wang, J. et al. Decadal Variability of Great Lakes Ice cover in response to AMO and PDO, 1963–2017. *J. Clim.* **31**, 7249–7268 (2018).
39. Abdelhady, H. U. & Troy, C. D. A deep learning approach for modeling and hindcasting Lake Michigan ice cover. *J. Hydrol.* **649**, 132445 (2025).
40. Hansen, J., Ruedy, R., Sato, M. & Lo, K. Global surface temperature change. *Rev. Geophys.* **48**, 4004 (2010).
41. Austin, J. & Colman, S. A century of temperature variability in Lake Superior. *Limnol. Oceanogr.* **53**, 2724–2730 (2008).
42. Wang, J. et al. Temporal and spatial variability of Great Lakes ice cover, 1973–2010. *J. Clim.* **25**, 1318–1329 (2012).
43. Assel, R. A., Quinn, F. H. & Sellinger, C. E. Hydroclimatic factors of the recent record drop in Laurentian Great Lakes water levels. *Bull. Am. Meteorological Soc.* **85**, 1143–1151 (2004).
44. Anderson, E. J., Tillotson, B. & Stow, C. A. Indications of a changing winter through the lens of lake mixing in Earth’s largest freshwater system. *Environ. Res. Lett.* **19**, 124060 (2024).
45. Piccolroaz, S., Toffolon, M. & Majone, B. The role of stratification on lakes’ thermal response: the case of Lake Superior. *Water Resour. Res.* **51**, 7878–7894 (2015).
46. Bai, X., J., W., C., S., A., C. & R., A. The impacts of ENSO and AO/NAO on the interannual variability of Great Lakes ice cover. Tech. Rep., NOAA Great Lakes Environmental Research Laboratory (2010).
47. Lin, Y. C., Fujisaki-Manome, A. & Wang, J. Recently amplified interannual variability of the Great Lakes Ice cover in response to changing teleconnections. *J. Clim.* **35**, 6283–6300 (2022).
48. McPhaden, M. J. Genesis and evolution of the 1997–98 El Nino. *Science* **283**, 950–954 (1999).
49. Assel, R. A. The 1997 ENSO event and implication for North American Laurentian Great Lakes winter severity and ice cover. *Geophys. Res. Lett.* **25**, 1031–1033 (1998).
50. Anderson, E. J. et al. Seasonal overturn and stratification changes drive deep-water warming in one of Earth’s largest lakes. *Nat. Commun.* **12**, 1–9 (2021).
51. Gronewold, A. D. et al. Coasts, water levels, and climate change: a Great Lakes perspective. *Climatic Change* **120**, 697–711 (2013).
52. Saber, A., Cheng, V. Y. & Arhonditsis, G. B. Evidence for increasing influence of atmospheric teleconnections on water levels in the Great Lakes. *J. Hydrol.* **616**, 128655 (2023).
53. Bai, X., Wang, J., Sellinger, C., Clites, A. & Assel, R. Interannual variability of Great Lakes ice cover and its relationship to NAO and ENSO. *J. Geophys. Res.: Oceans* **117**, 3002 (2012).
54. Giamalaki, K. et al. Signatures of the 1976–1977 Regime Shift in the North Pacific Revealed by Statistical Analysis. *J. Geophys. Res.: Oceans* **123**, 4388–4397 (2018).
55. Xue, P. et al. Enhancing Winter Climate Simulations of the Great Lakes: Insights from a New Coupled Lake-Ice-Atmosphere (CLIAv1) Model on the Importance of Integrating 3D Hydrodynamics with a Regional Climate Model (2024).
56. Notaro, M. et al. Cold season performance of the NU-WRF regional climate model in the Great Lakes region. *J. Hydrometeorol.* **22**, 2423–2454 (2021).
57. Xiao, C., Lofgren, B. M., Wang, J. & Chu, P. Y. Improving the lake scheme within a coupled WRF-lake model in the Laurentian Great Lakes. *J. Adv. Modeling Earth Syst.* **8**, 1969–1985 (2016).
58. Large, W. G. & Pond, S. Open ocean momentum flux measurements in moderate to strong winds. *J. Phys. Oceanogr.* **11**, 324–336 (1981).
59. Fairall, C. W., Bradley, E. F., Hare, J. E., Grachev, A. A. & Edson, J. B. Bulk parameterization of air-sea fluxes: Updates and verification for the COARE algorithm. *J. Clim.* **16**, 571–591 (2003).
60. Charusombat, U. et al. Evaluating and improving modeled turbulent heat fluxes across the North American Great Lakes. *Hydrol. Earth Syst. Sci.* **22**, 5559–5578 (2018).
61. Hunke, E. C. & Dukowicz, J. K. An elastic-viscous-plastic model for sea ice dynamics. *J. Phys. Oceanogr.* **27**, 1849–1867 (1997).
62. Yang, T. Y., Kessler, J., Mason, L., Chu, P. Y. & Wang, J. A consistent Great Lakes ice cover digital data set for winters 1973–2019. *Sci. Data* **7**, 1–12 (2020).
63. Li, X. et al. Climate change threatens terrestrial water storage over the Tibetan Plateau. *Nat. Clim. Change* **12**, 801–807 (2022).
64. Higgins, S. I., Conradi, T. & Muhoko, E. Shifts in vegetation activity of terrestrial ecosystems attributable to climate trends. *Nat. Geosci.* **16**, 147–153 (2023).
65. Bigi, A. & Harrison, R. M. Analysis of the air pollution climate at a central urban background site. *Atmos. Environ.* **44**, 2004–2012 (2010).
66. Deng, Q. & Fu, Z. Comparison of methods for extracting annual cycle with changing amplitude in climate series. *Clim. Dyn.* **52**, 5059–5070 (2019).
67. Seabold, S. & Perktold, J. Statsmodels: Econometric and statistical modeling with python. In *9th Python in Science Conference* (2010).
68. Virtanen, P. et al. SciPy 1.0: Fundamental Algorithms for Scientific Computing in Python. *Nat. Methods* **17**, 261–272 (2020).

69. Roberts, R. A. & Mullis, C. T. *Digital signal processing* (Addison-Wesley Longman Publishing Co., Inc., 1987).
70. Smith, K. L. *Climate and Geophysical Data Analysis Course* (University of Toronto Scarborough, 2020).
71. Wu, Z. & Huang, N. E. Statistical significance test of intrinsic mode functions. *Hilbert-huang Transform And Its Applications* 107–127 (2005).
72. Wunsch, C. Bermuda sea level in relation to tides, weather, and baroclinic fluctuations. *Rev. Geophysics* **10**, 1–49 (1972).
73. Press, W. H. Flicker noises in astronomy and elsewhere. *Modern Physics, Part C-Comments on Astrophysics* **7** (1978).
74. Prieto, G. multitaper: a multitaper spectrum analysis package in Python. *Seis. Res.* (2022).
75. Donald B., P. & Walden, A. T. *Spectral analysis for physical applications*. (Cambridge University Press, 1993).
76. Biltoft, C. A. & Pardyjak, E. R. Spectral coherence and the statistical significance of turbulent flux computations. *J. Atmos. Ocean. Technol.* **26**, 403–409 (2009).

Acknowledgements

This research is supported by the National Science Foundation (NSF OCE 2319044) and National Oceanic and Atmospheric Administration awarded to Cooperative Institute for Great Lakes Research (CIGLR) through the NOAA Cooperative Agreement with the University of Michigan (NA22OAR4320150). A.D.G. and H.U.A. also received support from the NSF Global Centers program (Award No. 2330317). J.W. was supported by NOAA OAR Ocean Sciences Portfolio “Great Lakes Earth System Model” project. This is CIGLR contribution 1262 and GLERL contribution 2076.

Author contributions

H.U.A. led and coordinated the various components of the study. H.U.A., A.F.M., and D.C. configured the hydrodynamic-ice model. H.U.A. designed and performed the data analysis. H.U.A., A.F.M., D.C., A.G., J.W. discussed the results, aided in their interpretation and contributed in writing the paper.

Competing interests

The authors declare no competing interests.

Additional information

Supplementary information The online version contains supplementary material available at <https://doi.org/10.1038/s43247-025-02341-x>.

Correspondence and requests for materials should be addressed to Hazem U. Abdelhady.

Peer review information *Communications Earth & Environment* thanks the anonymous reviewers for their contribution to the peer review of this work. Primary Handling Editors: Kyung-Sook Yun and Alireza Bahadori. A peer review file is available.

Reprints and permissions information is available at <http://www.nature.com/reprints>

Publisher's note Springer Nature remains neutral with regard to jurisdictional claims in published maps and institutional affiliations.

Open Access This article is licensed under a Creative Commons Attribution 4.0 International License, which permits use, sharing, adaptation, distribution and reproduction in any medium or format, as long as you give appropriate credit to the original author(s) and the source, provide a link to the Creative Commons licence, and indicate if changes were made. The images or other third party material in this article are included in the article's Creative Commons licence, unless indicated otherwise in a credit line to the material. If material is not included in the article's Creative Commons licence and your intended use is not permitted by statutory regulation or exceeds the permitted use, you will need to obtain permission directly from the copyright holder. To view a copy of this licence, visit <http://creativecommons.org/licenses/by/4.0/>.

© The Author(s) 2025